Dual mode of PGRP-LE-dependent NF-κB pathway activation in bacteria infected guts

Manish Joshi, Annelise Viallat-Lieutaud and Julien Royet*

Aix-Marseille Université, CNRS, IBDM-UMR7288, Turing Center for Living Systems, 13009 Marseille, France.

* Corresponding authors: e-mail julien.royet@univ-amu.fr

Abstract

Some of the interactions between prokaryotes and eukaryotes are mediated by a molecular dialogue between microbial MAMPs and host PRRs. Bacteria-derived peptidoglycan, which possesses all the characteristics of a MAMP, is detected by membrane-bound or cytosolic PRRs belonging to various families of proteins in both animals and plants (PGRP, Nod, Lys-M...). If the identity and the epistatic relationship between the downstream components of the signaling cascades activated upon PGN/PRR interactions are well characterized, little is known about the subcellular events requires to translate these early sensing steps into downstream target gene transcription. Using a model of *Drosophila* enteric infection, we show that gut-associated bacteria can induce PGRP-LE intracellular aggregation. Observed in both enterocytes and entero-endocrine cells, these aggregates were found to co-localize with the early endosome marker Rab5. *In vivo* functional analysis further demonstrates that, whereas some PGRP-LE target genes, such as antimicrobial peptides, can be activated independently of Rab5, other such as the PGRP-SC1 amidase, need the combine action of PGRP-LE and Rab5 to be transcribed.

These results demonstrate how by using different intracellular signaling routes, the same ligand/receptor complex can activate different target genes in the same cell.

Introduction

Since microbes and animals have co-evolved for millions of years, it is no surprise that bacteria deeply influence the biology of the host such as the developmental pattern they follow, the type of immunological response they trigger or even the behavior response into which they engage. Some of the prokaryotes/eukaryotes interactions are mediated by a molecular dialog between Microbe Associated Molecular Patterns (MAMPs) and host Pattern Recognition Receptors (PRRs). MAMPs are molecular signatures highly conserved in whole classes of microbes but absent from the host. Their recognition by germline-coded, intracellular and membrane-associated receptors, named PRR triggers *ad hoc* responses in the host. Bacterial PeptidoGlycaN (PGN) fulfilled all the characteristics of a *bone fide* MAMP[1, 2]. Also called murein, PGN is present in almost all bacterial species where it contributes to cell wall shape and integrity. PGN is glycan polymer of alternating β (1,4)-linked N-acetylglucosamine (GlcNAc) and N-acetylmuramic acid (MurNAc) residues that are cross-linked by short peptide bridges, the exact composition of which depends on the bacterial species and growth conditions. During bacterial proliferation, up to 50% of PGN is degraded by a turnover process that generates PGN fragments with a diverse structure known as muropeptides [3]. Their recognition by PRRs belonging to various classes of proteins family such Nod-like receptors (NLRs) and PeptidoGlycan Recognition Proteins (PGRPs) in animals and Lysine-motif (Lys-M) in plants is required to mobilize antibacterial host defenses but also to sustain developmental processes or activate behavior, to name just a few [4, 5, 6, 7, 8, 9, 10].

For few decades, *Drosophila melanogaster* serves as a model for studying aspects of the innate immunity that might otherwise be obscured by the actions of the adaptive immune response [11,

[12, 13, 14]. Previous work reveals that PGN detection by PGRP proteins explains many of the interactions that take place between flies and bacteria [15, 16, 17, 18]. While Di-AminoPimelic-type PGN (Dap-type PGN) is found in Gram-negative bacterial cell wall, Lysine-type PGN forms the cell wall of Gram-positive bacteria. When bacteria colonize the gut or enter the body cavity of a fly, they release PGN in the gut lumen or in the circulating insect blood. Detection of circulating Dap-type PGN by the membrane-associated PGRP-LC receptor expressed on immune cells (e.g. adipocytes and hemocytes) triggers an NF-kB/IMD-dependent production of immune effectors, such antimicrobial peptides (AMP), but also of regulators that controls the intensity of the immune response [19, 20, 21, 22, 23]. This PGN/PGRP-dependent NF-kB activation also takes place locally in the enterocytes that are in direct contact with gut microbiota. In some cells such as enterocytes, PGN is sensed intracellularly by the PGRP-LE cytosolic receptor that shares functional properties with the mammalian Nod2 PGN sensor [17, 24, 25, 26, 27, 28]. Interestingly, genetic data indicate that microbiota-born PGN can reach the insect blood where it activates NF-kB signaling in immune-competent cells and antagonized SREBP-dependent lipogenesis [29, 30]. More surprisingly, the same metabolite can also reach the brain where it modulates, in an NF-κB-dependent manner, the activity of some neurons, and hence modulate the behavior of infected flies [31, 32, 33].

Mainly via genetic and biochemical approaches, the epistatic relationship between the different components of the NF-kB signaling cascade, activated upon PGN sensing, has been elucidated with great details [34]. However, apart from the antimicrobial peptide transcriptional reporters[35], no molecular tools is available to visualize PGN sensing by PGRP and to follow subsequent activation of downstream NF-κB transducing mechanisms in cells. AMP reporters are only activated in some of the cells that sense PGN and are visible by microscopy much later that the onset of NF-κB activation measured by qRT-PCR on target genes such as AMP. In addition, they inadequat to follow PGN-mediated responses that are AMP-independent. To further

characterize PGN sensing and transducing events, we generated via the CRISPR/cas9 technology, flies carrying endogenous tagged versions of the cytosolic PGN receptor PGRP-LE. Microscopic and genetics characterization of these chimeric proteins allowed us to demonstrate that PGRP-LE-dependent PGN sensing and transducing mechanisms in enterocytes occurs at least via two modes, only one of them depending on the early depending on the early endosome marker, Rab5.

Results

Generating tools to visualize PGRP-LE-dependent NF-κB signaling *in vivo*

In order to visualize PGN sensing and signaling events *in vivo*, and at the cellular and subcellular levels, we engineered transgenic flies in which the PGRP-LE sensor was fused either to a V5 epitope or to an eGFP protein (Fig 1A). While the V5 tag was inserted between the PGRP domain and the cRHIM motif of PGRP-LE, the eGFP protein was added at the C-term end of the PGRP-LE locus (Fig 1A). In these flies, transcription of either PGRP-LE::V5 or PGRP-LE::GFP loci is regulated by the endogenous promoter and all the PGRP-LE proteins produced are tagged. To test whether these proteins could be detected *in vivo*, guts from PGRP-LE::V5 and PGRP-LE::GFP were orally infected with *Erwinia carotovora carotovora (E.cc)*, a strong activator of the NF-κB signaling cascade in the gut and in remote tissues [36]. The staining corresponding to V5 or eGFP was barely detectable in guts of flies raised on conventional medium. However, in flies fed for 6 hours with *E.cc*, PGRP-LE::V5 was detected as aggregates all along the midgut (except in the R5 domain) with a strong accumulation in R4, a domain previously shown to be almost fully PGRP-LE-dependent as far as NF-κB pathway activation is concerned (Figs 1B-D)[17]. These aggregates were also detected in guts of PGRP-LE::GFP infected flies (S Figs 1A, B). To ensure that the V5 staining corresponds to PGRP-LE protein only, staining was performed in clones of cells in which PGRP-LE was down-regulated

via RNAi. In cells in which PGRP-LE mRNA levels were efficiently reduced, PGRP-LE aggregates were no longer observed, in contrast to wild type neighboring cells (Figs 1E, S1B). Consistently, guts in which PGRP-LE was ubiquitously downregulated (using the Mex-Gal4 driver), no longer activated NF-κB pathway upon *E.cc* infection, as quantified by *AttacinD* transcription (Figs 1F, G). To test whether aggregates accumulation was a consequence of an increase of PGRP-LE transcription following infection or related to the transgenes, mRNA levels of PGRP-LE were quantified in wild-type, PGRP-LE::V5, and PGRP-LE::GFP and PGRP-LE^{112} backgrounds. Neither of these transcript levels were affected upon infection compared to control (Fig 1H). This suggested that enteric bacterial infection triggers the aggregation of PGRP-LE proteins already present in enterocytes before infection. A similar PGRP-LE clusterization was also observed in entero-endocrine cells, the second type of differentiated cells in the fly gut (S1 Fig C). We then tested whether the tags added to PGRP-LE affect their ability to sense and to transduce the PGN signal. As shown (Fig 1I), the inducibility of *AttacinD* transcripts upon *E.cc* oral infection remains similar in wild type *(w-)*, PGRP-LE::GFP and PGRP-L::V5 flies. Altogether these data demonstrate that the tools we generated to visualize PGRP-LE *in vivo* did not impair or modify the PGRP-LE-dependent immune response in the gut and that *E.cc* oral infection triggers PGRP-LE aggregation in intestinal cells.

PGRP-LE aggregation correlates with NF-κB pathway activation

To further understand/characterize the dynamics of PGRP-LE dependent NF-κB/Imd pathway in a temporal manner, time course oral infections were performed. As soon as one hour post infection, PGRP-LE aggregates were detected in R4 enterocytes (Figs 2A and B). The size and the number of PGPR-LE aggregates increased over time. However, while their number reached a maximum at 6hpi, and then decreased, they continuously grew reaching a maximum size at

24hpi (Figs 2A-C). Interestingly, the kinetic of PGRP-LE aggregation paralleled that of the NF-κB signaling pathway quantified via *AttacinD* transcription (Figs 2B and D). We then monitored aggregates formation in guts infected with *E. coli* and heat killed *E.cc* (*hk E.cc*) both poor inducers of the gut NF-κB signaling (Fig 2H). *E. coli*, which did not activate the NF-κB pathway, also did not induce PGRP-LE aggregates formation (Figs 2E-G). *hk E.cc* which induced a weak *AttacinD* transcription, induced a higher number of aggregates that alive *E.cc* although of smaller size (Figs 2E-H). Guts infected with commensal bacteria such as *Lactobacillus plantarum* [37] or *Acetobacter pomorum* [38] did not show any sign of PGRP-LE aggregation and were unable to activate *AttacinD* transcription (Figs 2I-L). Since PGRP-LE has been shown to directly bind Dap-type PGN, we tested the ability of PGN to induce PGRP-LE aggregation (Fig 2E). When fed to flies, pure *E. coli* PGN did not induce PGRP-LE clusterization. Since this treatment was also inefficient in triggering *AttacinD* transcription (Fig 2H), we hypothesized that the presence of PGN cleaving enzymes, such as lysozyme or amidases, in the gut lumen could degrade active PGN and hence explain its inability to trigger PGRP-LE clustering and, subsequently, NF-κB downstream signaling [39, 40, 41]. Collectively, these data demonstrated a strong correlation between the ability of a bacterial species to activate the NF-κB pathway and to trigger PGRP-LE clusterization

NF-κB, hedgehog signaling components and bacteria-derived uracil are not required for PGRP-LE aggregates formation

To further characterize PGRP-LE clusterization upon *E.cc* infection, we tested whether IMD pathway components were required to form these structures. Cells in which either the intracellular Fadd (Fas-Associated protein with Death Domain) adapter or the PGRP-LC receptor were down regulated via RNAi were still loaded with PGRP-LE aggregates upon *E.cc* infection, suggesting that these components were dispensable (Fig 3A). Since previous data

demonstrated that *E.cc*-derived uracil modulates DUOX-dependent gut immunity via hedgehog-induced Cad99C signaling endosomes, we tested the implication of bacteria-derived uracil and Hh signaling in PGRP-LE aggregation [42]. Hh signaling down-regulation (via Smo and Ci inactivation), did not interfere with the ability of *E.cc* to induce the formation of PGRP-LE aggregates (Fig 3B). Consistently, *E.cc* uracil auxotrophic mutants (*E. cc*$^{\Delta pyrE}$), that are unable to induce Cad99C endosomes, were as efficient as wild-type *E.cc* strains to induce PGRP-LE aggregate (Fig 3C). Furthermore, while uracil feeding had no effect on PGRP-LE aggregation, RNAi-mediated DUOX inactivation did not interfere with PGRP-LE aggregates formation upon *E.cc* infection (Fig 3 C, D). Therefore, bacterial uracil and the DUOX-related gut immunity do not seem to be required for the *E. cc*-induced PGRP-LE aggregates.

PGRP-LE aggregates are Rab5 positive but Rab7 negative

To determine the nature of PGRP-LE aggregates, we tested their relationship with subcellular compartments that forms the endocytic pathway. For that purpose, *E.cc*-infected guts were stained with antibodies against Rab5 and Rab7, two small GTPases usually associated with early and late endosomes[43 44]. One hour after infection, PGRP-LE aggregates did not colocalize with Rab5 (Fig 4A). Additionally, the number of detectable Rab5 positive structures increases with time and, by 3hpi, most PGRP-LE aggregates were positive for Rab5 reaching an almost complete colocalization by 6hpi (Figs 4A, B and 3B, C). Strikingly, no Rab5+/PGRP-LE- vesicles were observed suggesting that Rab5 and PGRP-LE are functionally linked (Fig 4A and B). In addition, none of the PGRP-LE vesicles colocalized with the late endosome marker Rab7 (Fig 4C). Furthermore, Rab5+/PGRP-LE+ vesicles were only poorly colocalized with another marker for early endosomes, Hrs (Fig 4D). As for PGRP-LE aggregates, *E. coli* was also unable to induce the formation of Rab5 and Hrs positive structures (Fig 4D). Colocalization between PGRP-LE aggregates and Rab5 prompted us to test the functional relationship between Rab5

and PGRP-LE and their downstream NF-κB/Imd pathway activation. Next, we tested the functional relationship between Rab5 and PGRP-LE by analyzing how reducing the level of one will affect the presence of the other. Cells in which PGRP-LE levels were reduced, still able to form Rab5 positive vesicles (Fig 4E). However, enterocytes of *E.cc*-infected guts in which Rab5 was down-regulated via RNAi, displayed abnormal PGRP-LE aggregates (Fig 4F). The PGRP-LE aggregates of Rab5 RNAi flies were more numerous and three times bigger than those in control animals (Fig 4G and H). As shown in Figs 2E-G, while *hk E.cc* induces numerous and rather smaller PGRP-LE aggregates, compared to live *E. cc* infection. Interestingly, while the live *E.cc*-induced clusters were Rab5 positive, the ones triggered in *hk E.cc* infected guts were not (Fig S2 C). These results suggest that although smaller PGRP-LE aggregates can form normally in the absence of Rab5, the latter is required for proper bigger *E.cc* mediated PGRP-LE aggregates. This is suggestive of a situation where *hk* or live *E.cc* can induce the formation of PGRP-LE aggregates and that only live *E.cc* triggers the association with Rab5 putatively leading to other properties for these clusters.

Rab5 is required for activation of only a fraction of NF-κB dependent target genes

Since Rab5 protein get associated with PGRP-LE in a kinetic that parallels that of NF-κB signaling, we wonder whether Rab5 plays a role in PGRP-LE-dependent NF-κB signaling. To test this hypothesis, we monitored PGRP-LE-dependent *AttacinD* transcription in the guts of *E.cc*-infected flies in which Rab5 levels were reduced. To our surprise, while RNAi-mediated PGRP-LE inactivation strongly impaired *AttacinD* mRNA inducibility, this was not the case in guts with reduced levels of Rab5 (Fig 5A). Since amidases such as PGRP-LB and PGRP-SC1 are also PGRP-LE-dependent target genes in the gut, we tested their putative regulation by Rab5. In contrast to what was observed with *AttacinD*, transcription of PGRP-SC1 was affected not only be reducing PGRP-LE levels but also by downregulating Rab5 in the gut (Fig 5D).

This effect was specific since it was not the case for PGRP-SC2 and PGRP-LB (Figs 5C, E). Since gut amidases have been shown to buffer gut lumen PGN levels and hence its diffusion to the hemolymph [15, 45], we tested the consequences of gut Rab5 inactivation on NF-kB activation in the remote fat body of *E.cc* infected flies. As reported before, flies in which PGRP-LE was only inactivated in the midgut presented an exacerbated fat body NF-κB activation following oral infection [17]. A similar phenotype was observed in flies with reduced levels of Rab5 in the gut (Fig 5B). To ensure that this phenotype was not secondary to a gut leakage associated with Rab5 or PGRP-LE inactivation, we performed the "smurf" assay[46]. As the blue dye remained confined in the intestinal tract, we concluded that excessive NF-κB activation in the fat body was not due to an intestinal barrier dysfunction (Fig 5F). Furthermore, while PGRP-SC1 downregulation in the gut did not affect local *AttacinD* transcription (Fig 5G, H), it phenocopies the exacerbated fat body immune response observed when reducing PGRP-LE or Rab5 levels in the gut. Thus, the association of PGRP-LE and Rab5 in the gut following *E.cc* exposure is necessary for the local induction of PGRP-SC1 that will impact the immune response of the remote fat body. However, this Rab5/PGRP-LE association is dispensable for a proper local antimicrobial response of the intestine. These results reinforced a model whereby Rab5 is required to selectively activate PGRP-LE-dependent target genes such as the PGRP-SC1 amidase.

Discussion

Using locus directed tagged-versions of PGRP-LE, we showed, for the first time, that bacterial-derived PGN induced PGRP-LE aggregation in enterocytes and entero-endocrine cells. Furthermore, the ability of a given species to trigger NF-κB seems to be linked to its ability to induce PGRP-LE clusterisation. These results are in good agreement with previous data showing that some muropeptides can induces infinite head-to-tail dimerization of PGRP-LE[47].

Whether these structures are related to the amyloid aggregates described earlier as signaling components of the IMD signaling is not clear and not easily testable [19]. Time course experiments and immunochemistry staining suggest a model in which PGN induce the formation of small cluster of PGRP-LE in enterocytes. When they reach a certain size, these PGRP-LE aggregates recruit the Rab5 protein. The fact that Rab5+/PGRP-LE+ vesicles do not transform into Rab7 positive structures over time, and that no Rab5 -/PGRP-LE+ are detected, suggest that they might not correspond to classic early endosomes. Alternatively, PGRP-LE might be continuously uploaded onto newly formed Rab5 endosomes. Our data demonstrate that two PGRP-LE-dependent transducing mechanisms cohabit in the enterocytes and enteroendocrine cells. PGRP-LE can signal independently of Rab5 to activate the transcription of some target gene such as *AttacinD or PGRP-LB* but required Rab5 to regulate the production of some target genes such as PGRP-SC1. This suggest that Rab5 containing vesicles can serve as signaling platform for PGRP-LE. Interestingly endosomes have been shown to be specialized platforms for bacterial sensing and NOD2 signaling and the endocytic pathway is required for the second *Drosophila* NF-kB innate immune signaling, Toll [48, 49 42]. Other organelles such as mitochondria or peroxisomes have been shown to be signaling platforms [50, 51]. Why should such a binary system necessary to respond to a single ligand-receptor interaction? It is conceivable that such a system would allow flies to respond to different thresholds of peptidoglycan and thus, potentially, of bacterial load. A low level of PGN would induce AMP production via PGRP-LE but independently of Rab5 while a high level of PGN, synonymous with a high infection, would require the production of a negative regulator to avoid the deleterious and documented effects of overactivation of the NF-kB pathway already reported [40, 52].

It is interesting to note that among all Gram-negative bacteria tested, and therefore all having a Dap-Type PGN in their cell wall, only *E.cc* was able to induce the formation of PGRP-LE+/Rab5+ vesicles and that this property was thermolabile. In addition, Rab5 vesicles can be

formed in the absence of PGRP-LE. Although it is possible that *E.cc* derived-PGN or other *E. cc* metabolite is the trigger of Rab5 vesicles, one could imagine a model in which two different *E.cc*-derived signal that induce in one hand, PGRP-LE vesicles, and the other hand, Rab5. Further work will be needed to test this hypothesis.

Acknowledgments

We thank Emilie Avazeri and Tanguy Tchifteyan for help with experiments, Léo Kurz and Olivier Zugasti for comments on the manuscript. This work was supported by ANR BACNEURODRO (ANR-17-CE16-0023-01), ANR PEPTIMET (ANR-18-CE15-0018-02), Equipe Fondation pour la Recherche Médicale (EQU201903007783) and Institut Universitaire de France to J.R.

Author contributions

Conceptualization, J.R.; Methodology, M.J., A.L.V. and J.R..; Investigation, M.J., A.L.V.; Formal analysis, M.J. and J.R.; Writing – original draft, M.J. and J.R.; Writing – reviewing & editing, J.R.; Funding acquisition, J.R.; Supervision, J.R.

Figure Legends:

Figure 1:

(**A**) Schematic representation of PGRP-LE locus. The PGRP-LE::V5 and PGRP-LE::GFP were generated by inserting V5 (between PGRP-domain and cRHIM motif) and eGFP (at C-terminus) using CRISPR-Cas9 method. The exonic coding sequences are depicted in grey and non-coding sequences are shown in orange. V5 tag is shown in red and eGFP tag is marked with green. The PGRP domain and cRHIM motif in protein are shown in blue and magenta, respectively.

(**B**) Adult midguts from uninfected and infected flies. Immunofluorescence showing PGRP-LE::V5 (red) and DNA (blue). Different regions of the midgut marked from R1 to R5. Scale bar represents 200 µm.

(**C**) Confocal images of different midgut regions (R1 to R5) showing PGRP-LE::V5 (red) and DNA (blue) in uninfected and infected flies. Scale bars represent 20 µm.

(**D**) Mean fluorescence intensity of PGRP-LE::V5 quantified in R4 region. Values were normalized with uninfected and plotted as mean ± SD. ****$p < 0.0001$; Mann-Whitney test.

(**E**) Confocal images of control and PGRP-LE^{RNAi} clones of infected flies showing GFP (clones) in green, PGRP-LE::V5 oligomers in red and DNA in blue. Scale bars represent 5 µm.

(**F** and **G**) *AttacinD* and *PGRP-LE* mRNA levels in posterior midgut in infected flies upon downregulation of PGRP-LE. ****$p < 0.0001$; Unpaired t test.

(**H** and **I**) The mRNA levels of PGRP-LE (H) and AttacinD (I) of indicated genotypes infected flies. ns (non-significant), $p > 0.05$; *p % 0.05; ***p % 0.001; One-way ANOVA with Tukey's post-test.

Infected flies were orally infected with *E. cc* for 6 hours. Confocal images are shown from R4 region of posterior midguts (E). For qRT-PCR results, mRNA levels in infected w^- (control) flies were set to 100% and all other values were expressed as a percentage of this value. qRT-

PCR results are shown as means ± SD from posterior midgut of ten female flies per genotype from at least three independent experiments.

Figure 2:

(**A**) Confocal images of PGRP-LE::GFP oligomers from uninfected and infected flies with *E. cc* at different time points showing GFP in green and DNA in blue.

(**B** and **C**) Quantification of numbers and average size of PGRP-LE::GFP oligomers from uninfected and infected flies with *E. cc* at different time points. ns (non-significant), $p > 0.05$; ***p % 0.001; ****$p < 0.0001$; Kruskal-Wallis test.

(**D**) *AttacinD* mRNA levels of uninfected and infected flies with *E. cc* at different time point. ns (non-significant), $p > 0.05$; ***p % 0.001; Kruskal-Wallis test.

(**E**) Confocal images of PGRP-LE::GFP oligomers from uninfected and infected with live *E. cc.* hk *E. cc, E. coli,* and ingested with *E. coli* PGN. GFP is shown in green and DNA in blue.

(**F** and **G**) Quantification of numbers and average size of PGRP-LE::GFP oligomers from uninfected and infected with live *E. cc.* hk *E. cc, E. coli,* and ingested with *E. coli* PGN. ns (non-significant), $p > 0.05$; ****$p < 0.0001$; Kruskal-Wallis test (F) and Mann-Whitney test (G).

(**H**) *AttacinD* mRNA levels of uninfected and infected with live *E. cc.* hk *E. cc, E. coli,* and ingested with *E. coli* PGN. ns (non-significant), $p > 0.05$; **$p < 0.01$; Kruskal-Wallis test.

(**I**) Confocal images of PGRP-LE::GFP oligomers from uninfected and infected with *E. cc. A. pomorum, L. plantarum* showing GFP in green and DNA in blue.

(**J** and **K**) Quantification of numbers and average size of PGRP-LE::GFP oligomers from uninfected and infected with live *E. cc. A. pomorum, L. plantarum*. ns (non-significant), $p > 0.05$; ****$p < 0.0001$; Kruskal-Wallis test.

(**L**) *AttacinD* mRNA levels of uninfected and infected with *E. cc. A. pomorum, L. plantarum*. ns (non-significant), $p > 0.05$; *$p < 0.05$; Kruskal-Wallis test.

Infected flies were orally infected with indicated bacteria/condition for 6 hours. Confocal images are shown from R4 region of posterior midguts. Scale bars represent 5 µm. For qRT-PCR results, mRNA levels in uninfected flies were set to 1 and all other values were expressed as a fold of this value. qRT-PCR results are shown as means ± SD from posterior midgut of ten female flies per genotype from at least three independent experiments.

Figure 3:

(**A**) Control, $Fadd^{RNAi}$ and $PGRP\text{-}LC^{RNAi}$ clones of infection flies. Immunofluorescence showing GFP (clones) in green, PGRP-LE::V5 oligomers in red and DNA in blue.

(**B**) Control, Smo^{RNAi} and Ci^{RNAi} clones of infected flies. Immunofluorescence showing GFP (clones) in magenta, PGRP-LE::V5 oligomers in red, Rab5 in green and DNA in blue.

(**C**) Confocal images of uninfected, infected with *E. cc*^{WT}, *E. cc*ΔpyrE, and ingested with uracil shown in R4 region.

(**D**) Confocal images showing PGRP-LE::GFP in control and $Duox^{RNAi}$ of infected flies. GFP is shown in green and mCherry marks nucleus.

Infected flies were orally infected/ingested with indicated bacteria/conditions (C) and *E. cc* (A, B and D) for 6 hours. Confocal images are shown from R4 region of posterior midguts. Scale bars represent 5 µm.

Figure 4:

(**A**) Confocal images of infected flies at different time points showing PGRP-LE::GFP oligomers in green, Rab5 positive endosomes in red and DNA in blue. Scale bars represent 2 µm.

(**B**) Colocalization quantification of PGRP-LE::GFP oligomers with Rab5 positive endosomes of infected flies at different time points. Pearson's R coefficient values are plotted in violin plot. ****$p < 0.0001$; Kruskal-Wallis test.

(**C**) Confocal images of uninfected and infected flies showing PGRP-LE::V5 oligomers in red and Rab7 positive endosomes in green. DNA is stained with DAPI (blue). Scale bars represent 2 µm.

(**D**) Colocalization quantification of PGRP-LE::V5 oligomers with Rab7 positive endosomes in uninfected and infected flies. Pearson's R coefficient values are plotted in violin plot. ****$p < 0.0001$; Mann-Whitney test.

(**E**) Confocal images of *E. cc* and *E. coli* infected flies showing PGRP-LE::GFP oligomers in green, Rab5 positive endosomes in magenta, and Hrs in red. DNA is stained with DAPI (blue). Scale bars represent 5 µm.

(**F**) Control and PGRP-LE^{RNAi} clones infected flies. Immunofluorescence showing GFP (clones) in green, PGRP-LE::V5 oligomers in red, Rab5 positive endosomes in magenta and DNA in blue. Scale bars represent 5 µm.

(**G**) Confocal images showing PGRP-LE::GFP oligomers in control and Rab5^{RNAi}. Scale bars represent 5 µm.

(**H** and **I**) Numbers and average size quantification of PGRP-LE::GFP oligomers in control and Rab5^{RNAi} of infected flies. **$p < 0.01$; ***$p < 0.001$; Mann-Whitney test.

Infected flies were orally infected with *E. cc* and *E. coli* for 6 hours. Confocal images are shown from R4 region of posterior midguts.

Figure 5:

(**A**) *AttacinD* mRNA levels in posterior midgut of infected flies in indicated genotypes. ns (non-significant), $p > 0.05$; ***$p < 0.001$; One-way ANOVA with Dunnett's post-test.

(**B**) *Diptericin* mRNA levels in carcass (fat body) of infected flies in indicated genotypes. ns (non-significant), $p > 0.05$; ***$p < 0.001$; Kruskal-Wallis test

(**C**-**E**) mRNA levels of *PGRP-LB* (C), *PGRP-SC1* (D), and *PGRP-SC2* (E) of infected flies in indicated genotypes. ns (non-significant), $p > 0.05$; $^{**}p < 0.01$; $^{****}p < 0.0001$; One-way ANOVA with Dunnett's post-test.

(**F**) Intestinal integrity test (Smurf assay) of infected flies in indicated genotypes. Scale bar represents 20 mm.

(**G**) *AttacinD* mRNA levels in posterior midgut of infected flies in indicated genotypes. ns (non-significant), $p > 0.05$; Unpaired t test.

(**H**) *Diptericin* mRNA levels in carcass (fat body) of infected flies in indicated genotypes. ns (non-significant), $p > 0.05$; $^{*}p < 0.05$; Unpaired t test.

Infected flies were orally infected with *E. cc* for 6 hours. For qRT-PCR results, mRNA levels in infected control flies were set to 100% and all other values were expressed as a percentage of this value. qRT-PCR results are shown as means ± SD from posterior midgut of ten female flies per genotype.

Figure S1:

(**A**) Adult midguts from uninfected and infected flies. Immunofluorescence showing PGRP-LE::GFP (green) and DNA (blue). Scale bar represents 200 µm. R4 region of PGRP-LE::GFP flies from uninfected and infected flies. Scale bar represent 20 µm.

(**B**) Confocal images of control and PGRP-LE^{RNAi} clones in infected flies showing RFP (clones) in red, PGRP-LE::GFP oligomers in green and DNA in blue. Scale bars represent 5 µm.

(**C**) Confocal images of uninfected and infected flies showing PGRP-LE::GFP oligomers in green and anti-Prospero positive (entero-endocrine) cells in red and DNA is stained with DAPI in blue.

Figure S2:

(**A**) Confocal images of control and Rab7^{DN} clones in infected flies showing GFP (clones) in green, PGRP-LE::V5 oligomers in red and DNA in blue. Scale bars represent 5 µm.

(**B**) Confocal images of uninfected and infected flies showing PGRP-LE::V5 oligomers in red and LAMP1 in green. DNA is stained with DAPI (blue). Scale bars represent 2 µm.

(**C**) Confocal images of flies infected with live and hk *E. cc* showing PGRP-LE::GFP oligomers in green and Rab5 in red. DNA is stained with DAPI (blue). Scale bars represent 5 µm.

Experimental Model and subject details:

Drosophila culture media:

Adult female *Drosophila melanogaster* was used to perform all the experiments. Flies were grown at 25°C on a yeast/cornmeal medium in 12h/12h light/dark cycle-controlled incubators. For 1 L of food, 8.2g of agar (VWR, cat.#20768.361), 80g of cornmeal flour (Westhove, Farigel maize H1) and 80 g of yeast extract (VWR, cat.#24979.413) were cooked for 10 min in boiling water. 5.2g of Methylparaben sodium salt (MERCK, cat.#106756) and 4 ml of 99% propionic acid (CARLOERBA, cat.#409553) were added when the food had cooled down. For antibiotic treatment (ATB), standard medium was supplemented with Ampicillin, Kanamycin, Tetracyclin and Erythromycin at 50 µg/ml final concentrations.

Fly strains and genetics:

The following strains were used in this work: PGRP-LE::V5 (This work), PGRP-LE::GFP (This work), w^{1118} (BL# 3605) Mutant line: PGRP-LE$^{112, 53}$RNAi-Lines: UAS-PGRP-LE^{RNAi} (BL# 60038), UAS-Rab5^{RNAi} (BL# 67877), UAS-Duox^{RNAi} (BL# 38907), UAS-Smo^{RNAi} (VDRC# 9542), UAS-Ci^{RNAi} (VDRC# 105620), UAS-PGRP-LC^{RNAi} (BL# 33383), UAS-PGRP-SC1a^{RNAi} (BL# 57184), UAS-Rab7^{DN} (Kindly provided by David Strutt) UAS-Fadd$^{RNAi\ 54}$ (Kindly provided by P. Meier) Gal4 Lines: Mex-Gal4 (kindly provided by Yixian Zheng), Tub-Gal80^{ts} (BL# 7018) Clonal Analysis Lines: CoinFLP (BL# 59269) hsFLP (BL# 6), hsFLP ; ActfrtStopfrtGal4 , UAS-GFP (Kindly provided by Y. Graba and A. Saurin lab).

Flies of genotypes containing the Gal4/UAS/Gal80^{ts} constructs were reared at 21 °C and transferred to 29 °C for 48 hours before infection to allow the expression of the Gal4 transcription factor.

Bacterial species and Infection:

Following microorganism were used: *Erwinia carotovora carotovora 15 2141* (*E. cc*) (grown at 30°C), *E. coli* (grown at 37°C), *Acetobacter pomorum* (grown at 30°C), *Lactobacillus plantarum* strain WJL (grown at 37°C). Microorganisms were cultured overnight in Luria-Bertani (for *E.* cc and *E. coli*) MRS medium (for *L. plantarum* and *A. pomorum*).

Oral Infection: We used 3–5 days old adult female raised at 25°C in presence of ATB in the food. Flies were starved for two hours before infection for synchronized feeding. Bacterial cultures were centrifuged at 4,000 RPM for 10 min at room temperature. Cells were serially diluted in water and their concentration was determined by optical density (OD) measurement at 600 nm. The food solution was obtained by mixing a pellet of bacterial culture with a solution of 5% sucrose (50/50) and added to a filter disk (final OD_{600} = 100) that completely covered surface of the fly food. For *E.* cc heat inactivation, a solution of *E.* cc diluted (final OD_{600} = 100) in 2,5% Sucrose was incubated at 100°C for 10 minutes, then cool down before use. PGN (500 ug/ml) and Uracil (100 nM) were orally administered similar as bacterial infection.

Construct and transgenesis:

PGRP-LE::V5:

The PGRP-LE::V5 fusion protein transgenic fly line was obtained by inserting, *via* CRISPR mediated recombination, a V5-tag cDNA in the 3rd exon of PGRP-LE, upstream of the PGRP domain"TCTdetector".

The V5 single-stranded oligo DNA nucleotides donor (ssODN) was synthetized by Eurofins MWG

(GATGCATACACGTTAACCATAGGATACCGATTTCACTTACAGAATTCAAAATACC CAAGagcggtggtaagcctatccctaaccctctcctcggtctcgattctacgggtggcGAGCTGTgCGCCATCATT CCGCGCTCTTCGTGGCTAGCACAGAAGCCCATGGACGAG). The guide RNA (ATGATGGCGCACAGCTCCTT), was cloned into pCFD3–dU6:3 gRNA (Addgene, 49410). w^{1118}; attP2(nos-Cas9) embryos were injected with both V5 ssODN donor (100 ng/µl) and pCFD3-gRNA vector (100 ng/µl). G0 were crossed to the balancer stock Sqh/FM7. Each F1 was crossed again to the balancer stock Sqh/FM7. Then its gDNA was extracted and screened by PCR for V5 presence. Positive lines were confirmed molecularly by sequencing.

PGRP-LE::GFP:

A PGRP-LE::GFP fusion protein transgenic line was obtained by inserting, *via* CRISPR mediated recombination, the meGFP cDNA at the C-term end of the PGRP-LE protein. The vector donor BS PGRP-LE::GFP was obtained by cloning the meGFP cDNA flanked by 1kb of PGRP-LE homology arms into the Bluescript vector using the following primers: fw5'arm:CGGGCTGCAGGAATTCATAAGCAACTCCACGAACGT,
rv5'arm:CTCGCCCTTGCTCACTTGTTCCTCCTCCTCGATATTG;
fw3'arm:CAAGCACCGGTCCACGTGAGGGACAAAAGAAGAGCAC,
rv3'arm:GGGCCCCCCCTCGAGTGACCAAACGAATGCAGGAC.

A co-CRISPR strategy (targets: PGRP-LE and ebony e) was used to simplify the screening process (KaneNSetal,2017). Guide RNAs (PGRP-LE:TCGAGGAGGAGGAACAATGA; ebony: GCCACAATTGTCGATCGTCA) were cloned into pCFD3–dU6: 3 gRNA (Addgene, 49410).

w^{1118}; attP2{nos-Cas9} embryos were injected with donor (500 ng/µl BS PGRP-LE::GFP) and guide vectors (100 ng/µl pCFD3 PGRP-LE; 100 ng/µl pCFD3 ebony). G0 were crossed to the double balancer stock def w+/FM6; Sb/TM3Ser, e. Each F1 with ebony body color (chrIII: nosCas9* e / TM3Ser, e) was crossed to the balancer stock Sqh/FM7. Then its gDNA was

extracted and screened by PCR for GFP presence. Positive lines were confirmed molecularly by sequencing.

Quantitative Real-Time PCR:

RNA from dissected posterior midgut and abdominal carcass (n=10) was extracted with RNeasy Mini Kit. Three hundred nanograms of total-RNA was then reverse transcribed in 20 ul reaction volume using the Superscript III enzyme (Invitrogen) and random hexamer primers. Quantitative real-time PCR was performed on a CFX96 Real-Time PCR Detection System (BIO-RAD) in 96-well plates using the FastStart Universal SYBR Green Master (Sigma-Aldrich). The amount of mRNA detected was normalized to control rp49 mRNA values. Normalized data was used to quantify the relative levels of a given mRNA according to cycling threshold (Ct) analysis.

Immunofluorescence/Confocal imaging and image processing:

Protocol without antibody staining: Adult fly guts were dissected in ice cold PBS and fixed for 20 min in 4% paraformaldehyde on ice. After 3 washes (5 minutes each) in PBT (1XPBS + 0.1% Triton X-100), the guts were mounted in Vectashield (Vector Laboratories) fluorescent mounting medium, with DAPI. Images of posterior midgut (R4 region) were captured immediately after mounting with a LSM 880 Zeiss confocal microscope.

Protocol for antibody staining: Following antibodies were used: Primary antibodies: Mouse anti-V5 (1:500, Invitrogen, R960-25), Rabbit anti-V5 (1:500, Invitrogen, MA5-32053), Rabbit anti-Rab5 (1:500 Abcam, ab31261), Mouse anti-Rab7 (1:500, Abcam, ab50533), Rabbit anti-LAMP1 (1:500, Abcam, ab30687), Chicken anti-GFP (1:2000, Aveslabs, GFP-1020), , Mouse anti-Prospero (1:50, DSHB, MR1A). Secondary antibodies: Donkey anti-mouse AF568 (1:500, ThermoFisher Scientific, A10037), Donkey anti-mouse AF647 (1:500, Jackson ImmunoResearch, 715605151), Donkey anti-rabbit AF568 (1:500, ThermoFisher Scientific, A10042), Donkey anti-rabbit AF647 (1:500, ThermoFisher Scientific, A31573). Adult fly guts

were dissected in ice cold PBS, fixed for 20 min in 4% paraformaldehyde on ice and washed 3 times in PBT (1XPBS + 0.1% Triton X-100). Tissues were blocked for 2h in PBT + 3% bovine serum albumin (BSA; Sigma-Aldrich) and then incubated overnight with the primary antibodies, in a cold room, on shaker. After 3 washes in PBT, the dissected tissues were incubated 2h with secondary antibodies. The tissues were next rinsed three times in PBT and mounted in Vectashield (Vector Laboratories) fluorescent mounting medium, with DAPI. Images of posterior midgut (R4 region) were captured with a LSM 880 Zeiss confocal microscope. Some images were false colored for consistency with other images in the manuscript

Smurf assay: For Smurf assay 3% (v/v) colorant bleu (E133) was mixed with *E. cc* containing oral infection food. After 6 hpi flies were imaged on Zeiss Stereo Lumar V12 microscope.

Data analysis:

All images were quantified using Fiji software (available at imagej.nih.gov/ij). The detailed methodology for analysis of various parameters is described as follows.

Intensity quantification: Fiji software was used to define the region of interest (ROIs) of 150*150 pixels corresponding to approximately one enterocyte in posterior midgut (R4 region). Random five ROIs were selected using rectangle selection tool keeping nucleus (DAPI) in the center. The mean intensity measurement of PGRP-LE::GFP and PGRP-LE::V5 was then conducted using measure tool (ImageJ function: Analyze > Measure). In all experiments, genotypes were analyzed in parallel. Each experiment was repeated independently at least three times, and one representative quantification is shown. Data were normalized with uninfected and plotted fold change of normalized mean intensity.

Oligomers number and size quantification: ImageJ macro programs were used to quantify number and size of oligomers. Briefly, random five ROIs of 150*150 pixels were selected using rectangle selection tool keeping nucleus (DAPI) in the center. Next, threshold (ImageJ function:

Image > Adjust > Threshold) was set and converted to mask. Watershed (ImageJ function: Process > Binary > Watershed) was used to separate closed oligomers by one pixel and then number and size of oligomers were quantified with analyze particles tool (ImageJ function: Analyze particles). All the genotypes were analyzed in parallel in all experiments. Each experiment was repeated at least three times, and one representative quantification is shown.

Colocalization quantification: ImageJ macro program were used to quantify colocalization. Briefly, random five ROIs of 150*150 pixels were selected using rectangle selection tool keeping nucleus (DAPI) in the center. Next, threshold (ImageJ function: Image > Adjust > Threshold) was set and converted to mask. Watershed (ImageJ function: Process > Binary > Watershed) was used to separate closed oligomers by one pixel and then number of oligomers were quantified with analyze particles tool (ImageJ function: Analyze particles). These quantified oligomers were used to quantify colocalization with Rab5 and Rab7 positive endosomes using JACoP (Just Another Colocalization Plugin) plugin in imageJ. Pearson's R coefficient values were used to plot graphs.

Statistical analysis and graphics:

The Prism software (GraphPad) was used for statistical analyses. Biorender was used to make schematic.

References

1. Bastos, P.A.D., Wheeler, R. & Boneca, I.G. Uptake, recognition and responses to peptidoglycan in the mammalian host. *FEMS Microbiol Rev* **45** (2021).

2. Tosoni, G., Conti, M. & Diaz Heijtz, R. Bacterial peptidoglycans as novel signaling molecules from microbiota to brain. *Current opinion in pharmacology* **48**, 107-113 (2019).

3. Irazoki, O., Hernandez, S.B. & Cava, F. Peptidoglycan Muropeptides: Release, Perception, and Functions as Signaling Molecules. *Front Microbiol* **10**, 500 (2019).

4. Girardin, S.E. *et al.* Nod1 detects a unique muropeptide from gram-negative bacterial peptidoglycan. *Science* **300**, 1584-1587 (2003).

5. Schloffel, M.A., Kasbauer, C. & Gust, A.A. Interplay of plant glycan hydrolases and LysM proteins in plant-Bacteria interactions. *Int J Med Microbiol* **309**, 252-257 (2019).

6. Mesnage, S. *et al.* Molecular basis for bacterial peptidoglycan recognition by LysM domains. *Nat Commun* **5**, 4269 (2014).

7. Saur, I.M.L., Panstruga, R. & Schulze-Lefert, P. NOD-like receptor-mediated plant immunity: from structure to cell death. *Nat Rev Immunol* **21**, 305-318 (2021).

8. Royet, J. & Charroux, B. Mechanisms and consequence of bacteria detection by the Drosophila gut epithelium. *Gut Microbes* **4**, 259-263 (2013).

9. Royet, J., Gupta, D. & Dziarski, R. Peptidoglycan recognition proteins: modulators of the microbiome and inflammation. *Nat Rev Immunol* **11**, 837-851 (2011).

10. Grenier, T. & Leulier, F. How commensal microbes shape the physiology of Drosophila melanogaster. *Curr Opin Insect Sci* **41**, 92-99 (2020).

11. Buchon, N., Silverman, N. & Cherry, S. Immunity in Drosophila melanogaster--from microbial recognition to whole-organism physiology. *Nat Rev Immunol* **14**, 796-810 (2014).

12. Broderick, N.A. & Lemaitre, B. Gut-associated microbes of Drosophila melanogaster. *Gut Microbes* **3**, 307-321 (2012).

13. Lestradet, M., Lee, K.Z. & Ferrandon, D. Drosophila as a model for intestinal infections. *Methods Mol Biol* **1197**, 11-40 (2014).

14. Schneider, J. & Imler, J.L. Sensing and signalling viral infection in drosophila. *Dev Comp Immunol* **117**, 103985 (2021).

15. Charroux, B. *et al.* Cytosolic and Secreted Peptidoglycan-Degrading Enzymes in Drosophila Respectively Control Local and Systemic Immune Responses to Microbiota. *Cell Host Microbe* **23**, 215-228 e214 (2018).

16. Capo, F., Charroux, B. & Royet, J. Bacteria sensing mechanisms in Drosophila gut: Local and systemic consequences. *Dev Comp Immunol* **64**, 11-21 (2016).

17. Bosco-Drayon, V. *et al.* Peptidoglycan sensing by the receptor PGRP-LE in the Drosophila gut induces immune responses to infectious bacteria and tolerance to microbiota. *Cell Host Microbe* **12**, 153-165 (2012).

18. Leulier, F. *et al.* The Drosophila immune system detects bacteria through specific peptidoglycan recognition. *Nat Immunol* **4**, 478-484 (2003).

19. Kleino, A. *et al.* Peptidoglycan-Sensing Receptors Trigger the Formation of Functional Amyloids of the Adaptor Protein Imd to Initiate Drosophila NF-kappaB Signaling. *Immunity* **47**, 635-647 e636 (2017).

20. Neyen, C., Runchel, C., Schupfer, F., Meier, P. & Lemaitre, B. The regulatory isoform rPGRP-LC induces immune resolution via endosomal degradation of receptors. *Nat Immunol* **17**, 1150-1158 (2016).

21. Maillet, F., Bischoff, V., Vignal, C., Hoffmann, J. & Royet, J. The Drosophila peptidoglycan recognition protein PGRP-LF blocks PGRP-LC and IMD/JNK pathway activation. *Cell Host Microbe* **3**, 293-303 (2008).

22. Gottar, M. *et al.* The Drosophila immune response against Gram-negative bacteria is mediated by a peptidoglycan recognition protein. *Nature* **416**, 640-644 (2002).

23. Choe, K.M., Werner, T., Stoven, S., Hultmark, D. & Anderson, K.V. Requirement for a peptidoglycan recognition protein (PGRP) in Relish activation and antibacterial immune responses in Drosophila. *Science* **296**, 359-362 (2002).

24. Kurata, S. Extracellular and intracellular pathogen recognition by Drosophila PGRP-LE and PGRP-LC. *Int Immunol* **22**, 143-148 (2010).

25. Yano, T. *et al.* Autophagic control of listeria through intracellular innate immune recognition in drosophila. *Nat Immunol* **9**, 908-916 (2008).

26. Kaneko, T. *et al.* PGRP-LC and PGRP-LE have essential yet distinct functions in the drosophila immune response to monomeric DAP-type peptidoglycan. *Nat Immunol* **7**, 715-723 (2006).

27. Takehana, A. *et al.* Peptidoglycan recognition protein (PGRP)-LE and PGRP-LC act synergistically in Drosophila immunity. *EMBO J* **23**, 4690-4700 (2004).

28. Chevee, V., Sachar, U., Yadav, S., Heryanto, C. & Eleftherianos, I. The peptidoglycan recognition protein PGRP-LE regulates the Drosophila immune response against the pathogen Photorhabdus. *Microb Pathog* **136**, 103664 (2019).

29. Gendrin, M., Welchman, D.P., Poidevin, M., Herve, M. & Lemaitre, B. Long-range activation of systemic immunity through peptidoglycan diffusion in Drosophila. *PLoS Pathog* **5**, e1000694 (2009).

30. Charroux, B. & Royet, J. Gut-derived peptidoglycan remotely inhibits bacteria dependent activation of SREBP by Drosophila adipocytes. *PLoS Genet* **18**, e1010098 (2022).

31. Masuzzo, A., Montanari, M., Kurz, L. & Royet, J. How Bacteria Impact Host Nervous System and Behaviors: Lessons from Flies and Worms. *Trends Neurosci* **43**, 998-1010 (2020).

32. Masuzzo, A. *et al.* Peptidoglycan-dependent NF-kappaB activation in a small subset of brain octopaminergic neurons controls female oviposition. *Elife* **8** (2019).

33. Kurz, C.L., Charroux, B., Chaduli, D., Viallat-Lieutaud, A. & Royet, J. Peptidoglycan sensing by octopaminergic neurons modulates Drosophila oviposition. *Elife* **6** (2017).

34. Kleino, A. & Silverman, N. The Drosophila IMD pathway in the activation of the humoral immune response. *Dev Comp Immunol* **42**, 25-35 (2014).

35. Tzou, P. *et al.* Tissue-specific inducible expression of antimicrobial peptide genes in Drosophila surface epithelia. *Immunity* **13**, 737-748 (2000).

36. Basset, A. *et al.* The phytopathogenic bacteria Erwinia carotovora infects Drosophila and activates an immune response. *Proc Natl Acad Sci U S A* **97**, 3376-3381 (2000).

37. Storelli, G. *et al.* Lactobacillus plantarum promotes Drosophila systemic growth by modulating hormonal signals through TOR-dependent nutrient sensing. *Cell Metab* **14**, 403-414 (2011).

38. Shin, S.C. *et al.* Drosophila microbiome modulates host developmental and metabolic homeostasis via insulin signaling. *Science* **334**, 670-674 (2011).

39. Costechareyre, D. *et al.* Tissue-Specific Regulation of Drosophila NF-x03BA;B Pathway Activation by Peptidoglycan Recognition Protein SC. *J Innate Immun* **8**, 67-80 (2016).

40. Paredes, J.C., Welchman, D.P., Poidevin, M. & Lemaitre, B. Negative regulation by amidase PGRPs shapes the Drosophila antibacterial response and protects the fly from innocuous infection. *Immunity* **35**, 770-779 (2011).

41. Marra, A., Hanson, M.A., Kondo, S., Erkosar, B. & Lemaitre, B. Drosophila Antimicrobial Peptides and Lysozymes Regulate Gut Microbiota Composition and Abundance. *mBio* **12**, e0082421 (2021).

42. Lee, K.A. *et al.* Bacterial uracil modulates Drosophila DUOX-dependent gut immunity via Hedgehog-induced signaling endosomes. *Cell Host Microbe* **17**, 191-204 (2015).

43. Clague, M.J. & Urbe, S. The interface of receptor trafficking and signalling. *J Cell Sci* **114**, 3075-3081 (2001).

44. Jacomin, A.C., Fauvarque, M.O. & Taillebourg, E. A functional endosomal pathway is necessary for lysosome biogenesis in Drosophila. *BMC Cell Biol* **17**, 36 (2016).

45. Zaidman-Remy, A. *et al.* The Drosophila amidase PGRP-LB modulates the immune response to bacterial infection. *Immunity* **24**, 463-473 (2006).

46. Rera, M., Clark, R.I. & Walker, D.W. Intestinal barrier dysfunction links metabolic and inflammatory markers of aging to death in Drosophila. *Proc Natl Acad Sci U S A* **109**, 21528-21533 (2012).

47. Lim, J.H. *et al.* Structural basis for preferential recognition of diaminopimelic acid-type peptidoglycan by a subset of peptidoglycan recognition proteins. *J Biol Chem* **281**, 8286-8295 (2006).

48. Huang, H.R., Chen, Z.J., Kunes, S., Chang, G.D. & Maniatis, T. Endocytic pathway is required for Drosophila Toll innate immune signaling. *Proc Natl Acad Sci U S A* **107**, 8322-8327 (2010).

49. Nakamura, N. *et al.* Endosomes are specialized platforms for bacterial sensing and NOD2 signalling. *Nature* **509**, 240-244 (2014).

50. Dixit, E. *et al.* Peroxisomes are signaling platforms for antiviral innate immunity. *Cell* **141**, 668-681 (2010).

51. Banoth, B. & Cassel, S.L. Mitochondria in innate immune signaling. *Transl Res* **202**, 52-68 (2018).

52. Tavignot, R., Chaduli, D., Djitte, F., Charroux, B. & Royet, J. Inhibition of a NF-kappaB/Diap1 Pathway by PGRP-LF Is Required for Proper Apoptosis during Drosophila Development. *PLoS Genet* **13**, e1006569 (2017).

53. Kaneko, T. *et al.* Monomeric and polymeric gram-negative peptidoglycan but not purified LPS stimulate the Drosophila IMD pathway. *Immunity* **20**, 637-649 (2004).

54. Khush, R.S., Leulier, F. & Lemaitre, B. Immunology. Pathogen surveillance--the flies have it. *Science* **296**, 273-275 (2002).

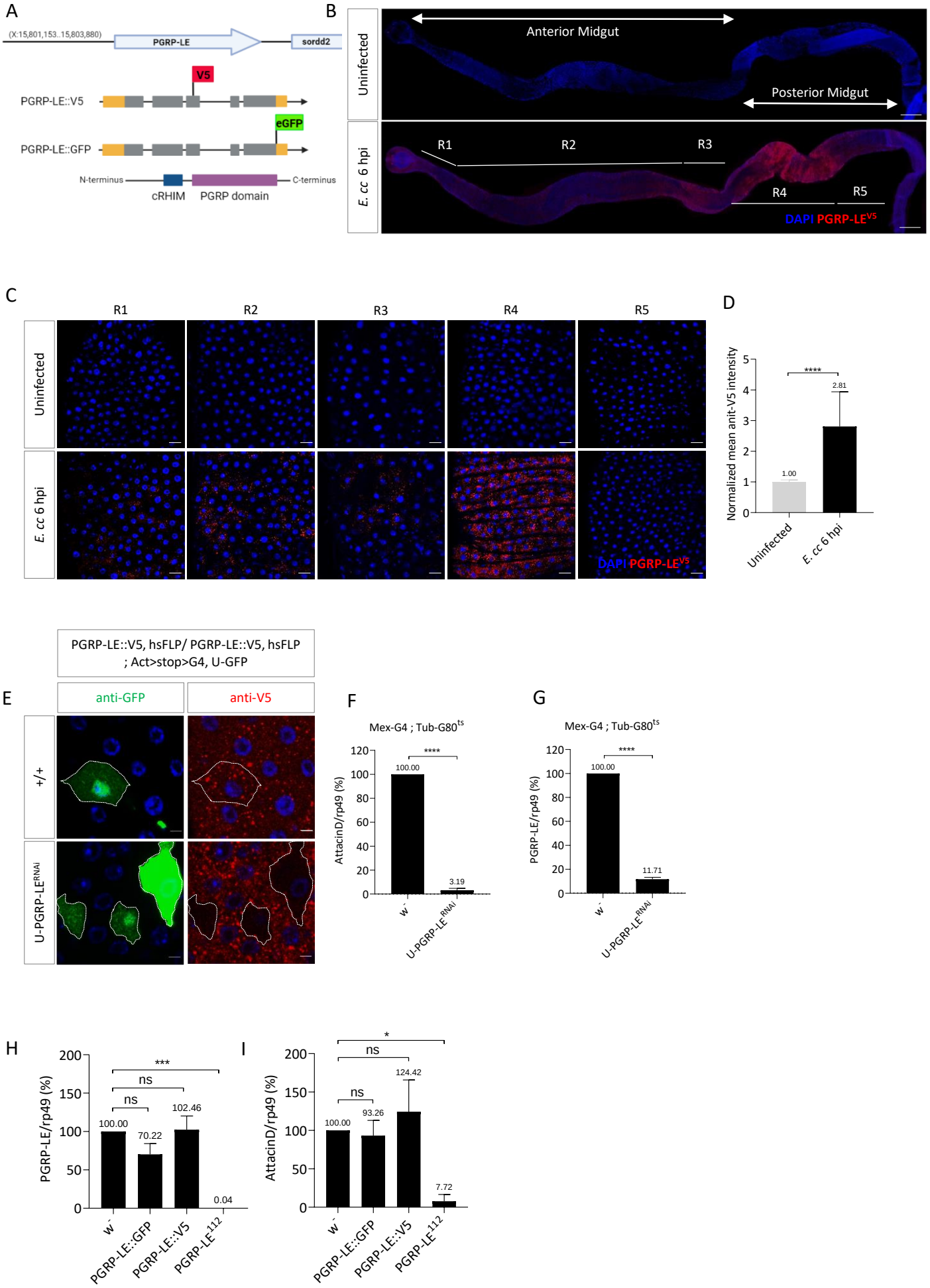
A
(X:15,801,153..15,803,880)
PGRP-LE
sordd2
V5
PGRP-LE::V5
eGFP
PGRP-LE::GFP
N-terminus
C-terminus
cRHIM
PGRP domain
B
Uninfected
Anterior Midgut
Posterior Midgut
E. cc 6 hpi
R1
R2
R3
R4
R5
DAPI PGRP-LE^V5
C
R1
R2
R3
R4
R5
Uninfected
E. cc 6 hpi
DAPI PGRP-LE^V5
D
Normalized mean anit-V5 intensity
****
2.81
1.00
Uninfected
E. cc 6 hpi
PGRP-LE::V5, hsFLP/ PGRP-LE::V5, hsFLP
; Act>stop>G4, U-GFP
E
anti-GFP
anti-V5
+/+
U-PGRP-LE^RNAi
F
Mex-G4 ; Tub-G80^ts
AttacinD/rp49 (%)
****
100.00
3.19
w-
U-PGRP-LE^RNAi
G
Mex-G4 ; Tub-G80^ts
PGRP-LE/rp49 (%)
****
100.00
11.71
w-
U-PGRP-LE^RNAi
H
PGRP-LE/rp49 (%)
***
ns
ns
100.00
70.22
102.46
0.04
w-
PGRP-LE::GFP
PGRP-LE::V5
PGRP-LE^112
I
AttacinD/rp49 (%)
*
ns
ns
100.00
93.26
124.42
7.72
w-
PGRP-LE::GFP
PGRP-LE::V5
PGRP-LE^112

Figure 1

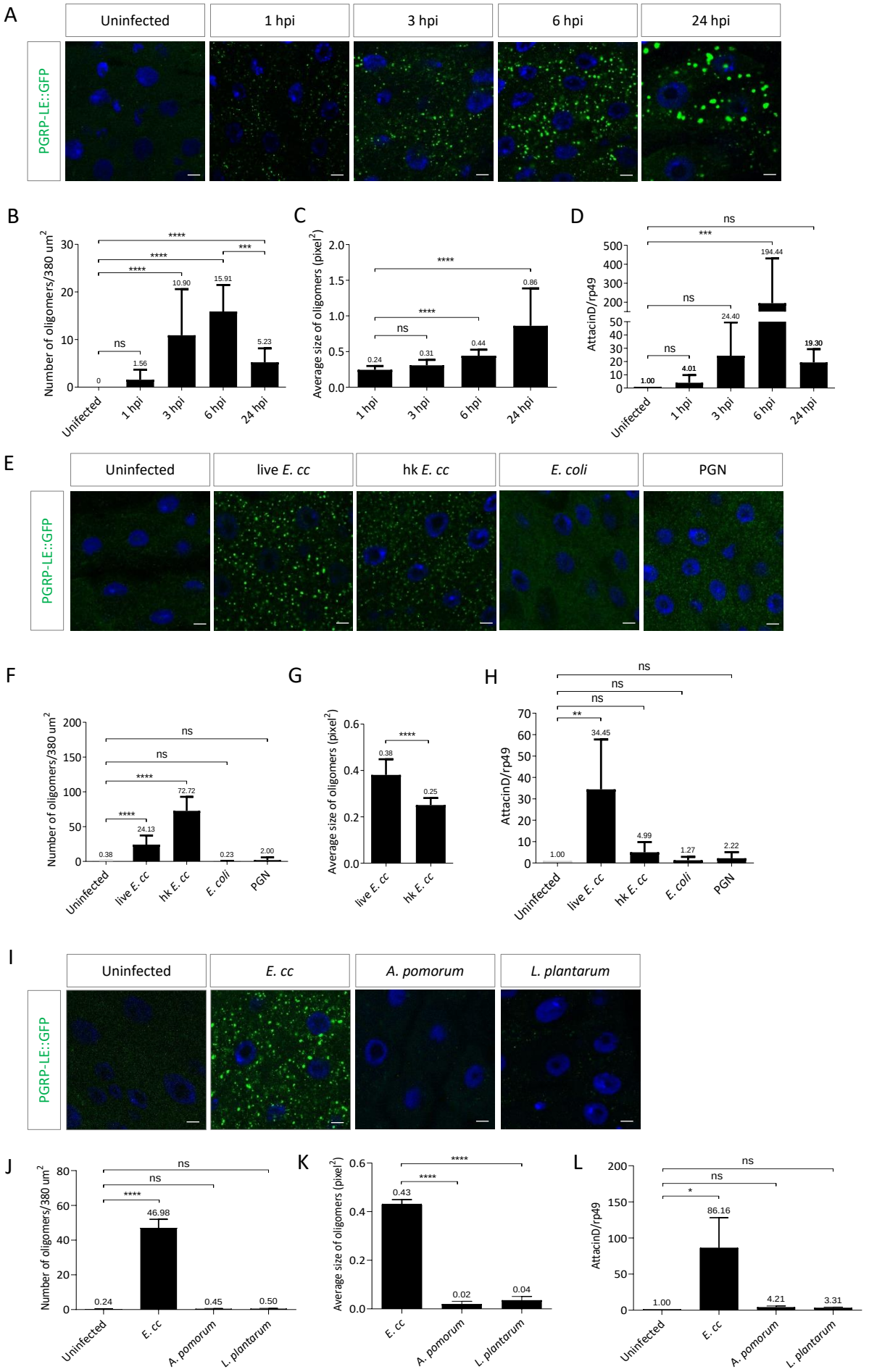
A
Uninfected
1 hpi
3 hpi
6 hpi
24 hpi
PGRP-LE::GFP
B
Number of oligomers/380 um2
0
1.56
10.90
15.91
5.23
ns
****
****
****
***
Unifected
1 hpi
3 hpi
6 hpi
24 hpi
C
Average size of oligomers (pixel2)
0.24
0.31
0.44
0.86
ns
****
****
D
AttacinD/rp49
1.00
4.01
24.40
194.44
19.30
ns
***
ns
ns
E
Uninfected
live E. cc
hk E. cc
E. coli
PGN
PGRP-LE::GFP
F
Number of oligomers/380 um2
0.38
24.13
72.72
0.23
2.00
ns
ns
****
****
Uninfected
live E. cc
hk E. cc
E. coli
PGN
G
Average size of oligomers (pixel2)
0.38
0.25
****
live E. cc
hk E. cc
H
AttacinD/rp49
1.00
34.45
4.99
1.27
2.22
ns
ns
ns
**
Uninfected
live E. cc
hk E. cc
E. coli
PGN
I
Uninfected
E. cc
A. pomorum
L. plantarum
PGRP-LE::GFP
J
Number of oligomers/380 um2
0.24
46.98
0.45
0.50
ns
ns
****
Uninfected
E. cc
A. pomorum
L. plantarum
K
Average size of oligomers (pixel2)
0.43
0.02
0.04
****
****
E. cc
A. pomorum
L. plantarum
L
AttacinD/rp49
1.00
86.16
4.21
3.31
ns
ns
*
Uninfected
E. cc
A. pomorum
L. plantarum

Figure 2

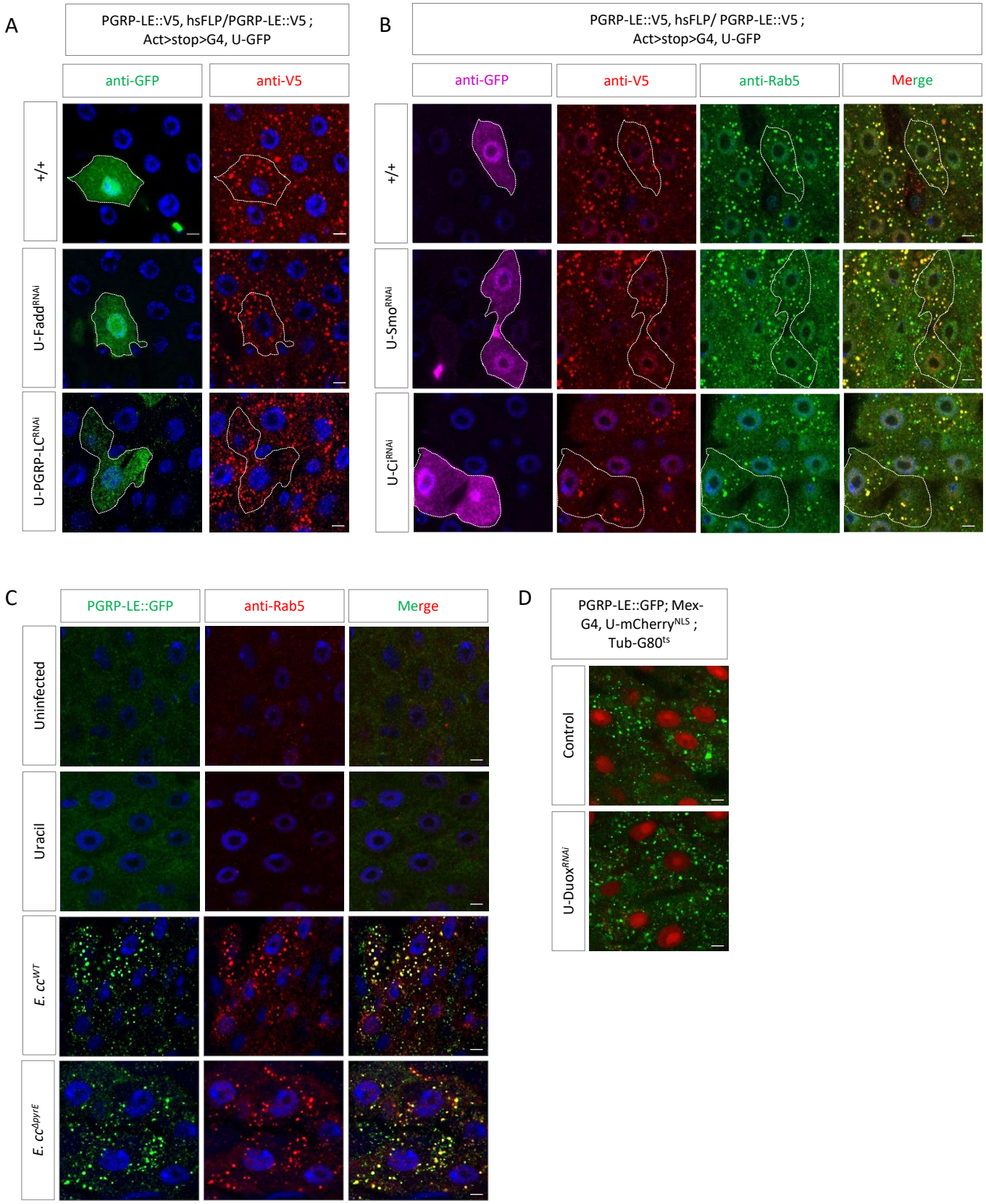
A
PGRP-LE::V5, hsFLP/PGRP-LE::V5 ;
Act>stop>G4, U-GFP
anti-GFP
anti-V5
+/+
U-Fadd^{RNAi}
U-PGRP-LC^{RNAi}
B
PGRP-LE::V5, hsFLP/ PGRP-LE::V5 ;
Act>stop>G4, U-GFP
anti-GFP
anti-V5
anti-Rab5
Merge
+/+
U-Smo^{RNAi}
U-Ci^{RNAi}
C
PGRP-LE::GFP
anti-Rab5
Merge
Uninfected
Uracil
E. cc^{WT}
E. cc$^{\Delta pyrE}$
D
PGRP-LE::GFP; Mex-G4, U-mCherry^{NLS} ;
Tub-G80^{ts}
Control
U-Duox^{RNAi}

Figure 3

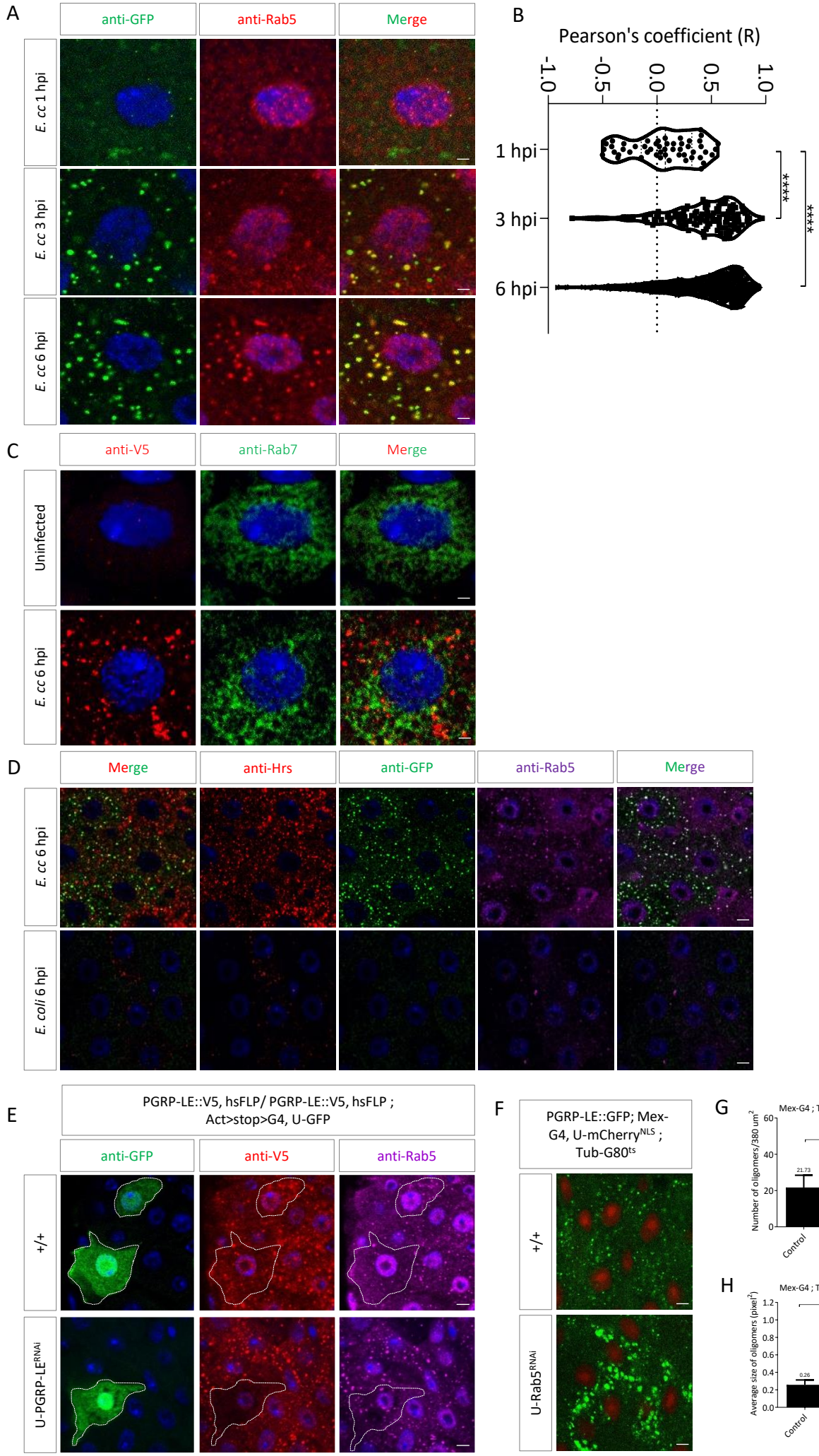
A
anti-GFP
anti-Rab5
Merge
E. cc 1 hpi
E. cc 3 hpi
E. cc 6 hpi
B
Pearson's coefficient (R)
-1.0
-0.5
0.0
0.5
1.0
1 hpi
3 hpi
6 hpi
****
****
C
anti-V5
anti-Rab7
Merge
Uninfected
E. cc 6 hpi
D
Merge
anti-Hrs
anti-GFP
anti-Rab5
Merge
E. cc 6 hpi
E. coli 6 hpi
E
PGRP-LE::V5, hsFLP/ PGRP-LE::V5, hsFLP ;
Act>stop>G4, U-GFP
anti-GFP
anti-V5
anti-Rab5
+/+
U-PGRP-LE^RNAi
F
PGRP-LE::GFP; Mex-G4, U-mCherry^NLS ;
Tub-G80^ts
+/+
U-Rab5^RNAi
G
Mex-G4 ; Tub-G80^ts
Number of oligomers/380 um^2
60
40
20
0
**
21.73
31.36
Control
U-Rab5^RNAi
H
Mex-G4 ; Tub-G80^ts
Average size of oligomers (pixel^2)
1.2
1.0
0.8
0.6
0.4
0.2
0.0
****
0.26
0.82
Control
U-Rab5^RNAi

Figure 4

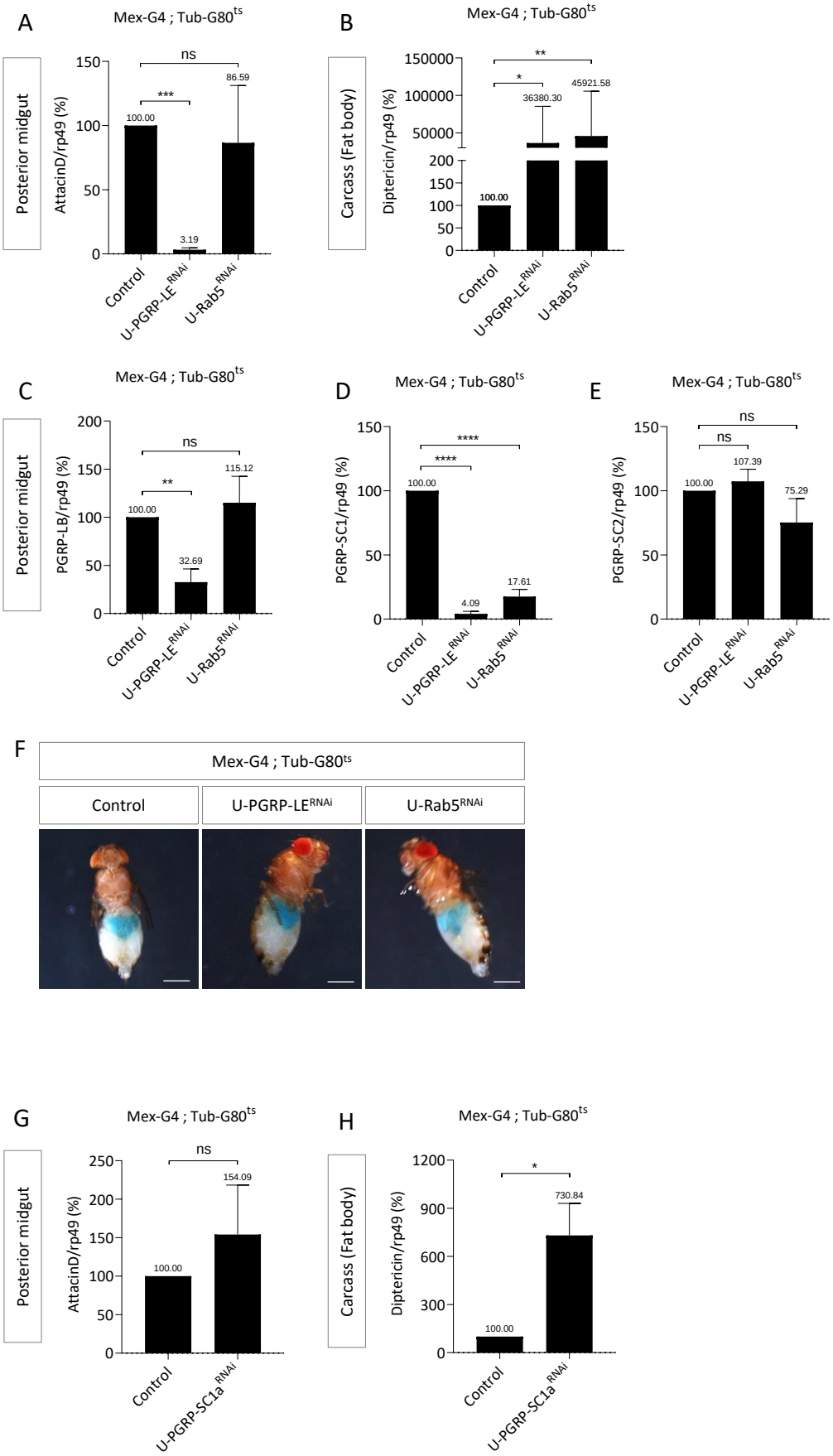
A
Mex-G4 ; Tub-G80ts
Posterior midgut
AttacinD/rp49 (%)
ns
***
100.00
3.19
86.59
Control
U-PGRP-LERNAi
U-Rab5RNAi
B
Mex-G4 ; Tub-G80ts
Carcass (Fat body)
Diptericin/rp49 (%)
**
*
36380.30
45921.58
100.00
C
Mex-G4 ; Tub-G80ts
Posterior midgut
PGRP-LB/rp49 (%)
ns
**
100.00
32.69
115.12
D
Mex-G4 ; Tub-G80ts
PGRP-SC1/rp49 (%)
****
****
100.00
4.09
17.61
E
Mex-G4 ; Tub-G80ts
PGRP-SC2/rp49 (%)
ns
ns
100.00
107.39
75.29
F
Mex-G4 ; Tub-G80ts
Control
U-PGRP-LERNAi
U-Rab5RNAi
G
Mex-G4 ; Tub-G80ts
Posterior midgut
AttacinD/rp49 (%)
ns
100.00
154.09
Control
U-PGRP-SC1a RNAi
H
Mex-G4 ; Tub-G80ts
Carcass (Fat body)
Diptericin/rp49 (%)
*
100.00
730.84
Control
U-PGRP-SC1a RNAi

Figure 5

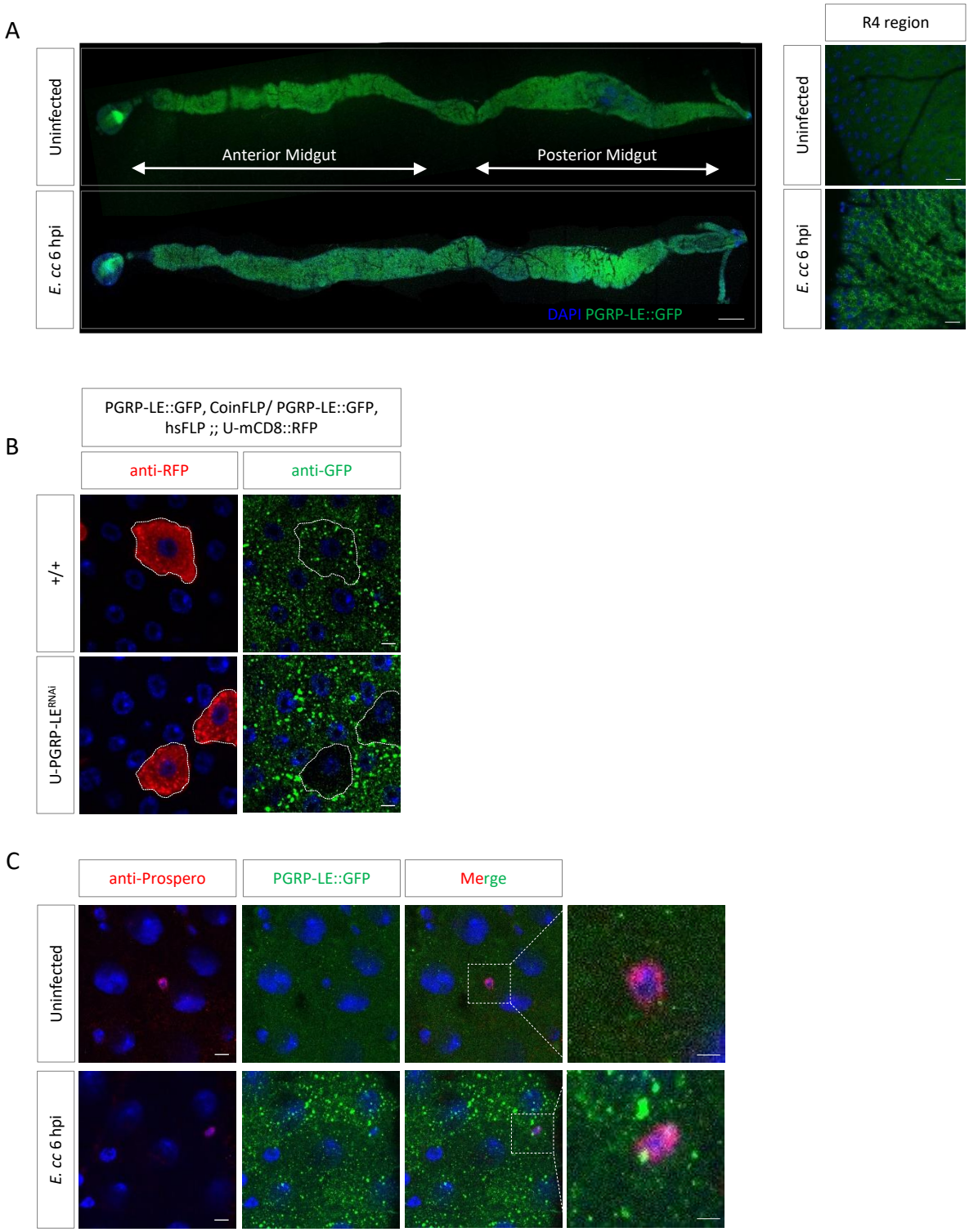
A
R4 region
Uninfected
Anterior Midgut
Posterior Midgut
E. cc 6 hpi
DAPI PGRP-LE::GFP
Uninfected
E. cc 6 hpi
B
PGRP-LE::GFP, CoinFLP/ PGRP-LE::GFP, hsFLP ;; U-mCD8::RFP
anti-RFP
anti-GFP
+/+
U-PGRP-LE RNAi
C
anti-Prospero
PGRP-LE::GFP
Merge
Uninfected
E. cc 6 hpi

Figure S1

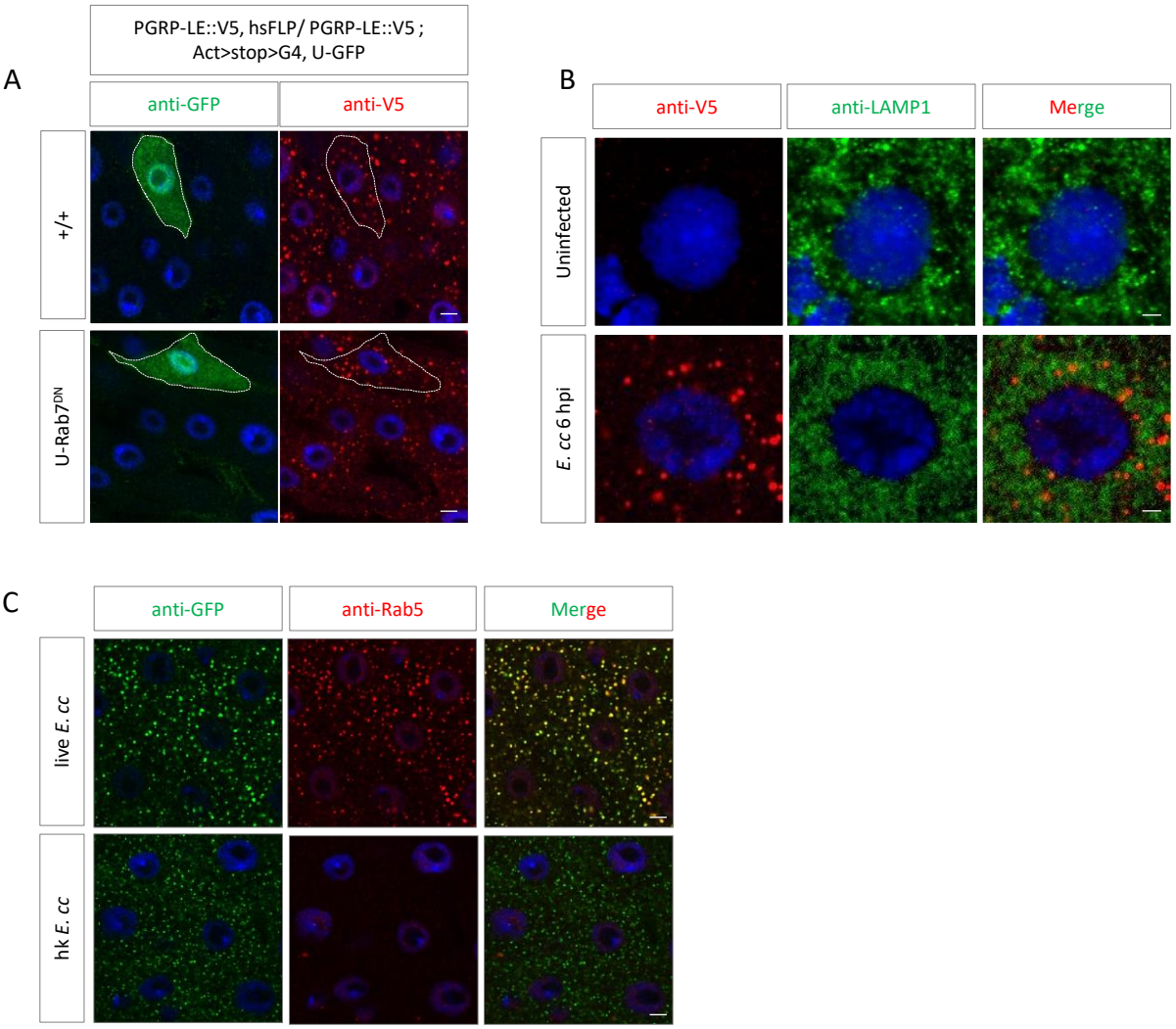
A
PGRP-LE::V5, hsFLP/ PGRP-LE::V5 ;
Act>stop>G4, U-GFP
anti-GFP
anti-V5
+/+
U-Rab7DN
B
anti-V5
anti-LAMP1
Merge
Uninfected
E. cc 6 hpi
C
anti-GFP
anti-Rab5
Merge
live E. cc
hk E. cc

Figure S2